Journal of Biomolecular NMR **29:** 21–35, 2004.

Interpretation of NMR relaxation properties of Pin1, a two-domain protein, based on Brownian dynamic simulations

Pau Bernadó[a,§], Miguel X. Fernandes[b], Doris M. Jacobs[c], Klaus Fiebig[c,‡], José García de la Torre[b] & Miquel Pons[a,*]

[a]*Departament de Química Orgànica, Universitat de Barcelona, Martí i Franquès 1-11, 08028 Barcelona, Spain and Laboratori de RMN de Biomolècules, Parc Científic de Barcelona, Josep Samitier 1-5, 08028 Barcelona, Spain;* [b]*Departamento de Química Física, Facultad de Química, Universidad de Murcia, 30071 Múrcia, Spain;* [c]*Institut für Organische Chemie und Chemische Biologie, Johann Wolfgang Goethe-Universität Frankfurt, Marie-Curie Str. 11, 60439 Frankfurt, Germany*

Received 25 August 2003; Accepted 26 November 2003

Key words: Brownian dynamics, multi-domain proteins, NMR relaxation, protein flexibility, reorientational mode dynamics, separation of global and local motions

Abstract

Many important proteins contain multiple domains connected by flexible linkers. Inter-domain motion is suggested to play a key role in many processes involving molecular recognition. Heteronuclear NMR relaxation is sensitive to motions in the relevant time scales and could provide valuable information on the dynamics of multi-domain proteins. However, the standard analysis based on the separation of global tumbling and fast local motions is no longer valid for multi-domain proteins undergoing internal motions involving complete domains and that take place on the same time scale than the overall motion.

The complexity of the motions experienced even for the simplest two-domain proteins are difficult to capture with simple extensions of the classical Lipari–Szabo approach. Hydrodynamic effects are expected to dominate the motion of the individual globular domains, as well as that of the complete protein. Using Pin1 as a test case, we have simulated its motion at the microsecond time scale, at a reasonable computational expense, using Brownian Dynamic simulations on simplified models. The resulting trajectories provide insight on the interplay between global and inter-domain motion and can be analyzed using the recently published method of isotropic Reorientational Mode Dynamics which offer a way of calculating their contribution to heteronuclear relaxation rates. The analysis of trajectories computed with Pin1 models of different flexibility provides a general framework to understand the dynamics of multi-domain proteins and explains some of the observed features in the relaxation rate profile of free Pin1.

Introduction

Inter-domain flexibility is an important issue for large multidomain proteins (Campbell and Downing, 1998) and is believed to be of functional importance in key biological processes involving protein-protein or protein-DNA recognition. For example, in calmodulin the N- and C-terminal domains, separated by a 27 residue linker, come together and clamp around target peptides (Ikura et al., 1992; Meador et al., 1993). Inter-domain flexibility is important to maintain a high affinity for a range of targets. FBP contains four K-homology repeats separated by linkers of various lengths and binds to single-stranded DNA (Burd and Dreyfuss, 1994). The NMR structure of a two-domain

‡Current address: Affinium Pharmaceuticals, 100 University Ave., 12th Floor North Tower, Toronto, Ontario, M5J 1V6, Canada.
§Current address: Institut de Biologie Structurale, Jean Pierre Ebel, 41 rue Jules Horowitz, 38027 Grenoble Cedex, France.
*To whom correspondence should be addressed. E-mail: mpons@ub.edu

construct bound to a 29-base single-stranded DNA fragment has been recently solved (Braddock et al., 2002), and the flexibility of the complex characterized both by measuring ^{15}N relaxation and by comparison of the alignment tensors of the two domains in diluted liquid crystalline medium. Complex flexibility is suggested to be an essential component of its function and changes in flexibility, induced by changing the length of the spacers have a direct effect on activity (Avigan et al., 1990). In fibrillin-1, an extracellular matrix protein comprising 43 calcium-binding epidermal growth factor-like modules and seven transforming growth factor β-binding protein-like modules, it has been found that a single mutation that changes inter-domain flexibility, but apparently has no other structural or protein life-cycle effects, is responsible for the Marfan syndrome phenotype (Yuan et al., 2002). SH2, SH3, WW and other domains that recognize short peptide fragments are often part of multidomain segments (Sicheri and Kuriyan, 1997), and such an arrangement may be related to their specificity, in which case inter-domain flexibility, including ligand-mediated inter-domain interactions, is expected to play a key functional role. A list of two-domain systems, with linkers of different lengths, studied by NMR using ^{15}N relaxation has been recently compiled (Yuan et al., 2002).

Structural characterization of multidomain proteins remains a challenge when the interaction between the domains is weak. Crystal structures of multidomain proteins with flexible linkers may be biased by packing forces, which are of the same magnitude of the inter-domain interactions. Conformational plasticity may sometimes be detected by the presence of different conformations in the unit cell or in different crystal forms (Gerstein and Krebs, 1998).

In solution, NOE-based methods based on short distance constraints usually do not provide enough information to accurately define the (average) relative orientation of the domains. In addition, multidomain proteins may experience large-scale dynamic processes. Conformational changes involving the relative motion of different domains may drastically change the overall shape of the protein and modulate its global tumbling.

The inclusion of long-range structural information, in the form of angular inter-vector constraints (Tolman et al., 1995; Tjandra et al. 1997), potentially alleviates the problem of domain orientation. However, angular constraints between distant bond vectors are obtained by reference to a common frame provided by the alignment tensor in anisotropic media (Fischer et al., 1999; Chou et al., 2001; Varadan et al., 2002) or the overall rotational diffusion tensor (Varadan et al., 2002; Brüschweiler et al., 1995; Fushman et al. 1999). These tensors are assumed to be characteristic of the structure studied and time independent. While fast local motion has little effect on these tensors, both become time dependent when large amplitude, low frequency inter-domain motions are present. In addition, alignment media can have an effect on the relative inter-domain orientation, especially when residue specific electrostatic interactions are involved (Fischer et al. 1999).

Methods based on relaxation measurements take advantage of anisotropic diffusion and have the potential of studying the dynamics of multidomain proteins in their native environment. Heteronuclear relaxation is sensitive to both internal and global motion and the different effects have to be separated. Parameters having completely different physical interpretation are mutually compensating, and failure to properly account for each of them may seriously compromise the accuracy of the others. These include the overall correlation time, roughly related to molecular size, the rotational diffusion anisotropy, related to molecular shape, and the different order parameters, related to molecular flexibility.

Separation of the different contributions is usually carried out on the basis of assumptions about their mutual independence (to separate overall and internal motions) or the predicted differential effects on the relaxation of nuclei belonging to bond vectors with different known orientations in the protein structure (to characterize anisotropy). However, the analysis of multidomain proteins is complicated by the fact that the usual basic assumption of independence between the overall and internal motions likely breaks down and the relative orientation of bonds in different domains is not known *a priori* and is probably time dependent.

There is no simple and rigorous method to extract inter-domain dynamics from experimental data. Recent advances in the analysis of the relaxation properties of multidomain or partially unfolded proteins include the use of an extended model free approach (Clore et al., 1990) that includes slow motion terms, common to all residues of each domain. The extended model-free approach provides a good approximation to the correlation function arising from a wobble-in-a-cone motional model, if the cone angle is small (Baber et al. 2001). For large cone angles, the slow and fast

order parameters and the time constant for the fast motions are overestimated and the time constant for the slow motion is underestimated (Chang and Tjandra, 2001).

For compact rigid molecules, internal motions can be separated from the overall reorientation of the molecule and simple functional forms are assumed to represent global tumbling. For flexible molecules, the internal motions modulate the shape and the global and internal motions are no longer separable and both have to be described simultaneously. Recently, Brüschweiler and coworkers have shown that the analysis of long molecular dynamic trajectories can be used to define collective reorientation eigenmodes, each possessing its internal correlation time (Prompers and Brüschweiler, 2001). Usually, individual snapshots are aligned to a reference structure to subtract the effects of global motion. If the alignment is omitted, global tumbling is accounted for by additional collective reorientation eigenmodes and the requirement of separability of internal and global motion can be removed. However, the conformational space should be sampled isotropically and the overall motion should be sampled for a time that is long with respect to the global correlation time, which is in the scale of tens of nanoseconds. The first limitation has been elegantly removed in the isotropic reorientation eigenmode dynamic analysis (iRED) (Prompers and Brüschweiler, 2002a). However, sufficiently long molecular dynamics in explicit solvent are still only possible for small molecules (Peter et al., 2001; Dagget, 2000).

Brownian dynamic (BD) simulations make use of hydrodynamic theory to predict the effect of collisions with solvent molecules and the friction exerted by the solvent on a moving particle (Allen and Tildesley, 1990). Hydrodynamic properties can be accurately calculated from the three dimensional structure of proteins or protein domains using shell methods (Carrasco and Garcia de la Torre, 1999a). By capturing only the essential surface features of the object and avoiding the use of explicit solvent Brownian dynamic simulations are computationally very efficient. A further simplification of the system can be obtained by using idealized models displaying hydrodynamic properties that are equivalent to the real object. In this way, Brownian Dynamic simulation can be extended to the microsecond time scale and are well suited to simulate global tumbling and large scale inter-domain motions that occur on the nanosecond time scale.

The peptidyl-prolyl cis-trans isomerase(PPIase) Pin1 is essential for cell cycle regulation and it consists of two domains separated by a 12 residue flexible linker: A N-terminal WW domain formed by 31 residues and a much larger C-terminal catalytic domain, 112 residues, which is structurally homologous to the FKBP-class of PPIases (Lu et al., 2002; Sekerina et al., 2000; Zhou et al., 1999). Pin1 selectively isomerizes peptides containing the sequence phospho-Ser/Thr-Pro. Peptides containing target sequences are recognized by both domains of the intact protein and also by the isolated WW domain. The isolated catalytic domain binds to some of the target peptides (e.g., WFYpSPR) but not to others (e.g., EQPLpTPVTDL) (Jacobs et al., 2003). Thus the two domains show a cooperative behavior in peptide binding.

The X-ray structure of Pin1 with a bound peptide has been reported (Verdecia et al., 2000). An additional X-ray structure contains a etilenglycol molecule bound to the peptide binding site (Ranganathan et al., 1997). In both structures the two domains are in contact while the linker is disordered.

The degree of interaction between the two domains of Pin1 in solution, both in the absence and in the presence of different peptide substrates, has been studied using NMR. A detailed study including the comparison of chemical shift of the individual domains and the full protein, the analysis of residual dipolar couplings in diluted liquid crystalline media and ^{15}N relaxation measurements have been published elsewhere (Jacobs et al., 2003).

In this article we present Brownian Dynamic simulations on different idealized models of Pin1. These calculations provide insight on issues such as the relative influence of direct inter-domain interactions versus spacer-induced restraint and the effect of hydrodynamic interactions on the conformational distribution of Pin1. However, the most important information derived concerns the interplay between global and internal dynamics in Pin1 and, in general in modular proteins formed by two domains separated by a flexible spacer. It is clear from the simulations that intramolecular domain-domain interactions are essential to understand global tumbling in flexible modular proteins. Reorientation eigenmodes are derived from the simulation and used to derive the minimum set of collective motions that have to be used to analyze the slow components, global and internal, that contribute to the correlation functions, and therefore to heteronuclear relaxation rates. In spite of the crudeness of the model used, the simulations provide a reasonable explanation for the observed relaxation rates of Pin1 and confirm the usefulness of BD simulations to ac-

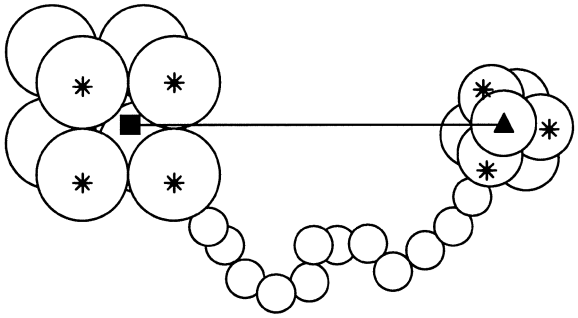

Figure 1. Schematic representation of the Pin1 model used for BD simulations. The square and triangle represent the pseudosymmetry axes of the domains that are collinear. Twelve identical strings between the beads marked with an asterisk were used to simulate direct domain-domain interactions. Non-interacting domains were represented by setting the force constant K to zero.

count for the slow components of relaxation, which can then be used to extract additional information on fast internal motions.

Methods

Hydrodynamic models of Pin1

Pin1 was modeled as two isotropic domains joined with a flexible linker. Each domain was analyzed individually, using the solid-state coordinates and HydroNMR in order to extract the expected correlation times for the individual domains. Using Stokes–Einstein equation, $\tau_C = 8\pi\eta_0 r^3/6kT$, where τ_c is the correlation time, η_0 is the viscosity of water at the working temperature T, 298 K, and k is the Boltzmann constant, it is possible to calculate the radius r of a sphere that would have the same correlation time as the real domain. A better numerical hydrodynamic description of a sphere is obtained when transformed to a cube made of eight tangent beads of radius $\sigma = 0.4668r$ (Garcia-Bernal and Garcia de la Torre, 1980; Carrasco and Garcia de la Torre, 1999b). This model can be understood as an intermediate state between the simple sphere and a detailed rough-shell bead model (Carrasco and Garcia de la Torre, 1999a). Final values of σ were 6.45 Å and 9.06 Å for the WW and catalytic domain respectively.

The equilibrium Pin1 model was obtained by arranging the two cubes vertex to face. That is, the cube representing the WW domain was placed with one of its C_3 axes collinear with one C_4 symmetry axis of the cube representing the catalytic domain. The flexible linker connected one of the four beads forming the face of the catalytic domain model that is in contact with the WW domain, and one of the three beads of the WW model that are tangent to the one that points directly to the large domain. The choice of the attachment points for the linker connecting the two domains roughly reproduces the topology of Pin1 observed in the X-ray structures. Figure 1 shows a schematic representation of the Pin1 model used in the simulations.

Residues in the flexible linker region were modeled as 3.8 Å tangent spheres with a fixed bond angle between three adjacent spheres of 146.4°. These parameters correspond to a poly-glycine chain (Levitt, 1976). The same parameter set had been used before to simulate a flexible loop of the triose phosphate isomerase (Wade et al., 1993). Torsion angles were left completely free. Trial runs using angular torsion potentials, as included in M. Levitt's force field (Levitt, 1976), provided indistinguishable results and torsion potentials were not included in the final simulations. Repulsive interactions were included between beads in both domains, between domains and linker and between bead i and beads farther than $i \pm 4$ in the linker chain. They were introduced as Lennard–Jones potencials (Levitt, 1976). The potential energy, ε, for beads belonging to domains was set to 0.236 kcal/mol that is the average of all residues of the Levitt's force-field. A 30 Å cutoff was used. No attractive interactions of any kind were introduced in the initial simulations. This model represents an upper bound for inter-domain flexibility in Pin1 and can provide insight on the constraints imposed by the covalent linkage between the two domains and the interference between hydrodynamic effects on the two tethered domains.

Experimental evidence, including differences in chemical shifts and relaxation rates between isolated domains and the complete protein, and the results from rigid body hydrodynamic models indicate that the two domains are interacting. This interaction was modeled by a set of twelve identical hookean strings between the two domains with a force constant K that was varied in different simulations to reproduce different degrees of coupling between the two domains. The strings connected the four beads forming the face of the catalytic domain model that is in contact with the WW domain, and the three beads of the WW model that are tangent to the one that points directly to the large domain.

In some simulations, only four strings were used, joining the four beads in the contact face of the cata-

lytic domain with a single bead along the symmetry axis of the WW domain. This arrangement allows free rotation around the inter-domain axis and can be used to test the restrictions imposed by the flexible linker. The use of multiple constraints restricts the relative rotation and the bending of the two domains much more effectively than the covalent linker and in several simulations the flexible linker was omitted to force average axial symmetry.

Simulation protocol

Brownian Dynamics simulations for a system of N particles are based on a generalized form of the Langevin equation, which states that the total force acting on each particle is the sum of three contribution: (a) The mechanical forces arising from the connection of the particle with other particles and eventually, the forces associated to external agents; (b) the frictional force, that is related not only to the velocity of that particle, but depends also on the velocity of all the other particles, due to the hydrodynamic interaction effect; and (c) in addition to the two previous deterministic components, there is also a stochastic force, typical of Brownian motion. For a full description of the Brownian dynamics with hydrodynamic interaction, see Ermak and McCammon (1978). The Langevin equation of N interacting particles is equation 6 in their paper.

Hydrodynamic interaction effects are potentially long range interactions that may be important when two particles, such as proteins or protein domains, approach each other (Brune and Kim, 1994; Antosiewicz and McCammon, 1995; Antosiewicz et al. 1996). Simulations without hydrodynamic interactions are convenient for comparative purposes. These simulations account for the effect of solvent in individual beads but do not take into account the influence of neighbor beads mediated by the solvent.

Ermak and McCammon (1978) derived an algorithmic solution of the generalized Langevin stochastic differential equation. The motion of the molecular model (the array of particles) is described by discrete time steps of duration Δt. If $\mathbf{r}_i^o$ is the initial position vector of the i-th bead (spherical particle), then its position after the time step , $\mathbf{r}'_i$, would be

$$\mathbf{r}'_i = \mathbf{r}_i^o + \frac{\Delta t}{k_B T}\sum_{j=1}^{N} \mathbf{D}_{ij}^o \cdot \mathbf{F}_j + \mathbf{R}_i^o, \tag{1}$$

where $\mathbf{F}_j$ is the mechanical and external force acting on bead j (forces of the kind (a) mentioned above), the 3×3 symmetric matrix $\mathbf{D}_{ij}^o$ is the ij component of the $3N\times3N$ diffusion tensor, and $\mathbf{R}_{ij}^o$ is a random vector with a covariance matrix given by:

$$\left\langle \mathbf{R}_i^o \cdot \mathbf{R}_j^o \right\rangle = 2\Delta t \mathbf{D}_{ij}^o. \tag{2}$$

The superscript 0 means that the quantity is referred to the initial position. The ii blocks are just the diffusion coefficient of the i-th bead:

$$\mathbf{D}_{ii} = \frac{k_B T}{\zeta_i}\mathbf{I} = \frac{k_B T}{6\pi\eta_o\sigma_i}\mathbf{I}, \tag{3}$$

where ζ_i is the friction coefficient of the bead, formulated according to the Stokes–Einstein law in terms of its radius σ_i and the solvent viscosity η_0. The hydrodynamic interaction effect is introduced through the ij components: the $\mathbf{D}_{ij}$ blocks are given by

$$\mathbf{D}_{ij} = k_B T \mathbf{T}_{ij}, \tag{4}$$

where $\mathbf{T}_{ij}$ is the hydrodynamic interaction tensor, which for pairs of identical beads can be computed using the Rotne–Prager–Yamakawa (Rotne and Prager, 1969; Yamakawa, 1970) modification of the Oseen tensor, which corrects for the non-pointlike nature of the frictional elements and correctly describes the possibility of overlapping, while when beads i and j have different radii (as it happens with our model; see Figure 1), $\mathbf{T}_{ij}$ is given by an extension of this tensor derived by Garcia de la Torre and Bloomfield (1981).

The Ermak–McCammon equation (1) is a first-order solution of the stochastic differential equation. It has been shown that there is a pseudo-second-order algorithm, in which each step is taken twice, in a predictor-corrector fashion proposed by Iniesta and Garcia de la Torre (1990). First a predictor step is taken according to Equation 1, finding a first approach for the final position, $\mathbf{r}'_i$. Then the step is repeated using forces and diffusion tensors that are the mean of those at $\mathbf{r}_i^o$ and $\mathbf{r}'_i$:

$$\mathbf{r}_i = \mathbf{r}_i^o + \frac{\Delta t}{k_B T}\frac{1}{2}\sum_{j=1}^{N}(\mathbf{D}_{ij}^o \cdot \mathbf{F}_j^o + \mathbf{D}'_{ij} \cdot \mathbf{F}'_j) + \mathbf{R}'_i. \tag{5}$$

Although each step requires more CPU time, this algorithm is slightly more efficient since it allows larger Δt and therefore requires a smaller number of steps.

Beads were kept in their tangential fixed conformation using hard hookean strings between each bead and all the neighboring ones, which gives identical results than the SHAKE algorithm but it is faster.

Starting from an extended conformation, 2 μs Brownian Dynamic simulations under different conditions were performed at 298 K with a time-step of

10 fs. Snapshots were recorded every picosecond for further analysis. The first 100 ns periods were not used for the analysis.

Results

Rigid body analysis of Pin1

The relaxation properties of proteins that behave as rigid bodies can be accurately computed from their three-dimensional structures using hydrodynamic calculations implemented in the HydroNMR program (Garcia de la Torre et al., 2000). The elementary atomic radius, a, is used in the program to generate a bead model of the protein. For non-aggregating rigid proteins, the experimental R_2/R_1 values are reproduced using a value of $a = 3.3$ Å, deviations from this value have been associated to aggregation ($a > 3.6$ Å) or to underlying large amplitude dynamics ($a < 2.9$ Å) (Bernado et al., 2002, 2003). Figure 2 shows that experimental R_2/R_1 values for Pin1 bound to peptide WFYpSPR in solution are reproduced to a good approximation using the X-ray structure of Pin1 (Ranganathan et al., 1997) with a value of $a = 3.3$ Å. This result indicates that Pin1 bound to WFYpSPR adopts a rigid structure in solution that is in good agreement with the reported solid-state structure of Pin1. On the other hand, experimental relaxation data from free Pin1 can only be approximately reproduced using the crystal structure and a value of $a = 2.5$ Å suggesting that free Pin1 shows considerable large scale motions in solution. In addition, the fitting of the N-terminal WW domain is poor and it would require still lower values of a. Again, the requirement of different a values for the two domains suggests inter-domain motion. However, the fact that experimental values could be reproduced using a solid-state structure by simply changing the value of a, suggests that the average free Pin1 structure retains some of the characteristic features of the rigid model. Therefore, one could envision the possibility of using a dynamic model based on the hydrodynamic properties of the solid-state structure, to try to reproduce the experimental values observed for Pin1 under different conditions.

The observed changes in experimental R_2/R_1 values suggest changes in the nanosecond time scale that could only be reproduced by molecular dynamic simulations expanding into the microsecond time scale. Therefore, we decided to use BD simulations, using the idealized model of Pin1 explained above, to explore the influence of different parameters in the calculated relaxation rates and to provide insight into plausible dynamic processes that could account for the observed experimental variations in relaxation rates in the presence or in the absence of bound peptides.

Free BD simulations

In order to characterize the statistical distribution of conformations of Pin1 allowed by the flexible linker but independent of direct attractive interactions between the two domains, we computed a 2 μs BD trajectory in which only repulsive interactions between non-bonded beads were considered. As a reference, an equivalent simulation without considering hydrodynamic interactions was calculated. In this simulation, solvent interactions for each bead are not affected by the presence of neighbor beads.

Figure 3 shows the variation of the relative position of the centers of the two domains along the two trajectories. The force field used in the BD simulations of Figure 3 does not include any attractive term. Inter-domain contacts are therefore the result of statistical fluctuations of the relative positions of the two domains modulated by the flexible connector and by hydrodynamic effects. A comparison of simulations with and without hydrodynamic interactions allows the separation of the two contributions.

The inclusion of hydrodynamic interactions clearly results in more compact structures, with a large number of snapshots showing distances lower than 40 Å, indicative of inter-domain contacts. The angular distribution in the presence of hydrodynamic interactions is narrower, with few conformations showing inter-domain angles larger than 90°. Histograms showing the distribution of inter-domain distances and inter-domain angles are shown as supplementary material.

Hydrodynamic interactions account for the fact that the force resulting from collisions of solvent molecules on a particular bead are affected by the presence of neighbor beads. This can be intuitively described as a ‘shadow effect’. A neighbor bead will act as an obstacle decreasing the probability of collision by solvent molecules approaching from that direction. Collisions with solvent molecules approaching from the opposite direction will be unhindered. Therefore, hydrodynamic effects will lead to compact structures, once the distance between the components becomes short enough. The fact that the two domains are covalently linked through a connector forces the two domains to remain at a distance where ‘solvent-

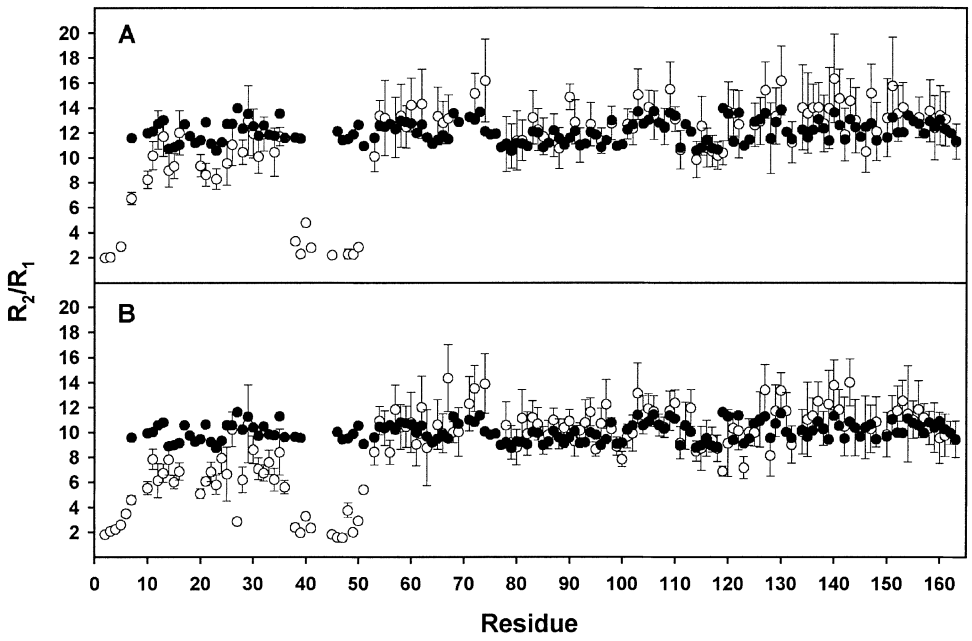

Figure 2. Comparison between experimental (open circles) and HydroNMR calculated (filled circles) R_2/R_1 ratios for peptide-loaded Pin1 (A) and free Pin1 (B). The same structure (pdb code: 1pin) was used in both cases. For peptide loaded Pin1 the standard value of a, 3.3 Å, was used but, in order to fit the experimental data, an unphysical low value of 2.5 Å had to be used for free Pin1.

shadowing' is effective and random solvent collisions tend to push the two domains together.

Rotational correlation times were computed for selected vectors as the average over the complete trajectory of $^1/_2$ $(3\cos^2\theta(\tau) - 1)$, where $\theta(\tau)$ the angle formed by the vector at times t and $t + \tau$. Figure 4 shows correlation functions of two orthogonal vectors in both the catalytic and WW domains of model Pin1 extracted from the simulation including hydrodynamic interactions. They are compared with the correlation functions expected from an axially symmetric ellipsoid calculated using the principal components of the rotational diffusion tensor derived from the three dimensional structure of the isolated catalytic domain using HydroNMR and with the results of Brownian Dynamic simulations on the isolated domains. The good agreement between the results from analytical hydrodynamic modeling using HydroNMR, and the analysis of the Brownian dynamic simulations shows the accuracy of the correlation times derived from the numerical simulations. The difference between the isolated domains and the complete system is larger for the WW domain, which is affected by the proximity of the larger domain. However, the fact that the correlation times of the individual domains in the Pin1 model without direct inter-domain attractive interactions are close to those of the isolated domains, indicate that inter-domain contacts induced by hydrodynamic interactions have very little effect on the reorientation of the individual domains.

Inter-domain constraints and the effect of the linker

Experimental correlation times of free Pin1 are longer than those of the isolated domains. This is obviously a consequence of inter-domain interactions not included in the simplest Pin1 model. Inter-domain interactions were simulated by including additional restrictions to the system in the form of a set of twelve identical strings, obeying Hooke's law with a force constant K, linking the two domains. The real situation is certainly much more complex involving short-range van der Waals interactions, long range electrostatic effects, and possibly equilibration processes between a conformational ensemble including 'open' conformations in which the relative orientation of the domains are not fixed and 'docked' conformation(s) in which the two domains adopt well defined conformations. In the presence of suitable peptide substrates, an additional equilibrium between peptide-free and peptide-bound Pin1 is also possible. Thus, inter-domain flexibility is expected to be strongly correlated with the

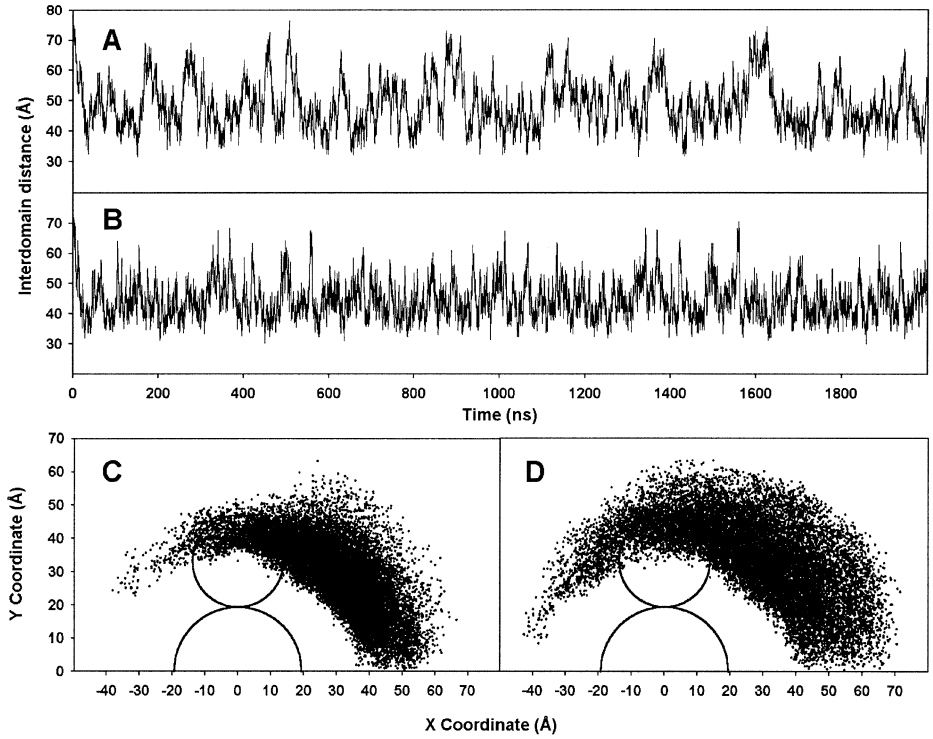

Figure 3. Relative positions of the two domains during free Brownian Dynamic simulations not including (A,D) or including (B,C) hydrodynamic interactions. No attractive interactions between domains were included. Plots A and B represent the distance between the centers of the two domains. Plots C and D indicate the position of the centre of the WW domain with respect to the catalytic domain every 100 ps. The attachment point of the flexible connector is on the positive direction of the X-axis. The angular distribution is axially symmetrical with respect to the X-axis and is reduced to the projection on the positive quadrant on the X-Y plane. Circles indicate the dimensions of the spheres that would have the same correlation times as the isolated domains.

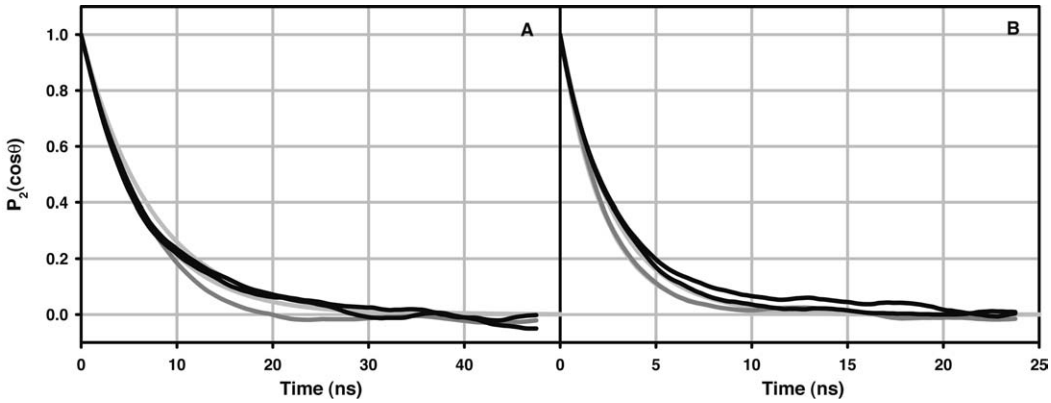

Figure 4. Autocorrelation functions of pairs of orthogonal vectors in the catalytic domain (A) and WW domain (B) of model Pin1 derived from 2 μs Brownian Dynamic trajectories are shown in black. Superimposed gray curves show autocorrelation functions of vectors aligned with D_{zz} and D_{yy} of the rotational diffusion tensor of each domain calculated with HydroNMR with an *a* value of 3.30 Å and the autocorrelation function calculated from 2 μs simulation of model isolated domains, which are isotropic (dark grey).

time average of the inter-domain distance reflecting conformational fluctuations.

The *ad hoc* representation used in the simulations shares with the real system the correlation between inter-domain flexibility and average inter-domain distance. In addition, it is computationally inexpensive and depends on a single parameter, K, which can be varied systematically in different Brownian dynamic simulations. This allows the simultaneous exploration of the statistical distribution of the geometrical properties of the conformational ensemble generated, which can be described by order parameters, and the time dependence of the fluctuations, which give rise to autocorrelation functions and correlation times, that are directly related to heteronuclear NMR relaxation rates.

The addition of inter-domain constraints between domains, which are already connected through a linker, breaks the axial symmetry of the model and introduces a pseudo-cycle. To determine the effect of the linker in the presence of direct inter-domain interactions we have carried out two experiments. In the first one, the two domains were connected by hard ($K = 100$) strings forcing them into contact, but allowing free rotation around the inter-domain axis and two BD simulations, with and without the flexible linker, were compared. The distributions of the dihedral angle between two vectors, one from each domain, perpendicular to the inter-domain axis are not identical. However, the pseudo-cyclic structure alone does not strongly restrict the rotation along the inter-domain axis and, in the presence of inter-domain restraints that prevent domain rotation, the additional effects of the linker can be neglected.

In a second experiment we compared BD simulations of two rigid Pin1 models, constrained so that no relative domain motion was allowed and differing only by the presence or the absence of the flexible linker. The autocorrelation functions derived from the simulations show that the flexible linker has an effect on the overall rotation of the system, which is higher for rotations along the inter-domain axis. Figures showing the effect of the linker can be found in the supplementary material.

In spite of the fact that the omission of the linker has measurable effects on the observed dynamics, the study of the effect of inter-domain flexibility was carried out without the flexible linker. This is justified by the computational simplification and the higher symmetry of the system, as well as the overall degree of approximation of the model. We expect that the major effect of this simplification would be an increase in the apparent anisotropy, which is already overestimated in a model constructed without considering any complementarity of domain shapes.

Conformational distributions and order parameters

Table 1 show the average and standard deviation of the inter-domain distance along BD trajectories using different values of K. Increasing the force constant results in more compact (lower average inter-domain distances) and more rigid models (lower standard deviations of the distance). In addition, the relative orientation of the domains is also restricted and the maximum value and the amplitude of the angular distribution depend on the value of K, as shown in Figure 5. Two different angles, α and β defined in Figure 5, were analyzed. Assuming axial symmetry, the vectors defining these angles can be considered restricted to a plane. Angle α describes the rotation of the center of the small domain around the large one. Angle β measures the rotation of the small domain around its own center.

Both angular distributions could be adjusted to a Weibull distribution

$$\mathrm{P}(\theta) = \mathrm{a} \cdot \left(\frac{\mathrm{c}-1}{\mathrm{c}}\right)^{\frac{\mathrm{c}-1}{\mathrm{c}}} \cdot \mathrm{g}^{\mathrm{c}-1} \cdot \mathrm{Exp}\left(-\mathrm{g}^{\mathrm{c}} + \frac{\mathrm{c}-1}{\mathrm{c}}\right), \tag{6a}$$

where $\theta = \alpha$ or β, and

$$\mathrm{g} = \left| \frac{\mathrm{x}-\mathrm{x}_0}{\mathrm{b}} + \left(\frac{\mathrm{c}-1}{\mathrm{c}}\right)^{1/c} \right|. \tag{6b}$$

According to the Lipari and Szabo formalism (Lipari and Szabo, 1982a,b), the fitted distribution function corresponding to different values of K and different angular definitions were analytically integrated to provide a value for the corresponding order parameter

$$\mathrm{S}^2 = \left(\frac{4\pi}{5}\right) \sum_{\mathrm{l}=-2}^{\mathrm{l}=2} \int_{\mathrm{v}} \left| \mathrm{p}(\theta)\, \mathrm{Y}_{2,\mathrm{l}}(\theta, \phi)\, \mathrm{dv} \right|^2, \tag{7}$$

where $\mathrm{p}(\theta)$ is the continuous normalized probability distribution function of a vector. $\mathrm{Y}_{2,\mathrm{l}}(\theta, \phi)$ are the spherical harmonic of rank 2 and (θ, ϕ) are the polar angles that defines the orientation of vectors described in Figure 5. These order parameters illustrate the motional restriction of the small domain with respect to the large domain and, in contrast to bond-vector order

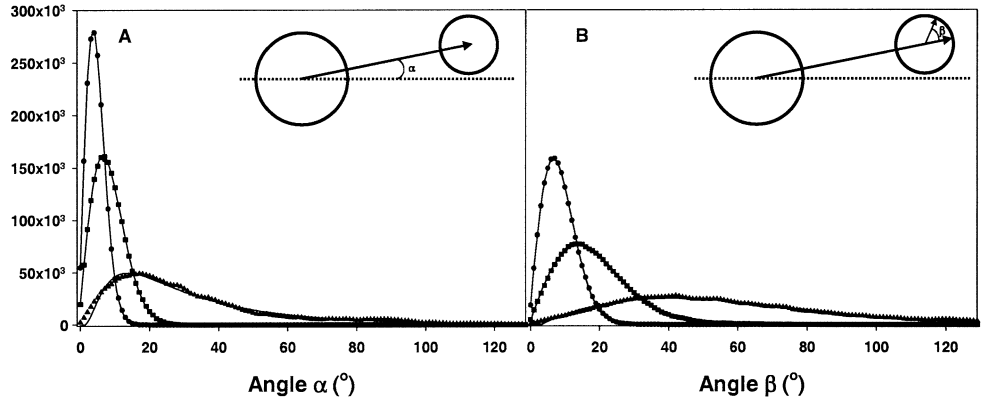

Figure 5. Definition and distribution of angles α (A) and β (B) for different values of K: 0.1 (circles), 0.025 (squares) and 0.0025 (triangles). Fitted distributions to equation 6 are shown in solid lines.

Table 1. Distance and derived order parameters in constrained BD simulations

Force constant K[a]	Average interdomain distance (Å)	S.D. of interdomain distance (Å)	[c]S^2_α	[c]S^2_β
10	28.61	0.41	1.00	1.00
0.1	31.07	0.92	0.96	0.87
0.075	31.41	1.00	0.95	0.83
0.05	31.93	1.15	0.93	0.75
0.025	33.17	1.45	0.88	0.54
0.01	35.39	2.06	0.76	0.18
0.0075	36.14	2.30	0.71	0.09
0.0050	37.28	2.69	0.60	0.02
0.0025	39.64	3.43	0.09	0.00
0.001	42.77	5.00	0.00	0.00
0[b]	44.51	6.08	0.00	0.00

[a]Force constant in adimensional units.
[b]Corresponding to free Pin1 model simulation with flexible linker.
[c]α and β are defined in Figure 5.

parameters, they are not directly accessible by NMR relaxation. The results are presented in Table 1.

The two order parameters show a different dependence on the value of K. While S^2_α decreases slowly with K until $K = 0.0050$, S^2_β shows a sharp decrease at values of K below 0.025. This is consistent with the view that rotational diffusion of an individual domain can be larger than the reorientation of the vector joining the centers of the two domains, which is basically a translational motion. This is also the expected situation in a real two-domain protein with a long linker, like Pin1, where fast reorientation of the domains is only restricted when the two domains are in contact.

Collective motions

A collective description of protein motion has been recently introduced in terms of reorientation eigenmodes (Prompers and Brüschweiler, 2001). Here we provide a short overview of the method, which is clearly explained in the references given. Correlated reorientation of different vectors can be captured in the covariance matrix of spherical harmonics of rank L, $Y_{LM}(\Omega)$, evaluated at their respective directions. Relaxation active interactions can be expressed in terms of spherical harmonics of rank 2 and, in isotropic media, should be independent of M. Isotropic averaging is obtained naturally if the simulation is extended for a time which is much longer than the correlation time of the motions involved. Alternatively, it can be forced by including for each vector a set of spherical harmonics with $M = -L, \ldots, +L$ (Prompers and Brüschweiler, 2002a). Isotropic averaging leads to a substantial simplification of the covariance matrix and the relevant information is contained in the matrix M with elements

$$M_{kl} = \overline{P_L(\cos(\Omega_k - \Omega_l))}, \qquad (8)$$

where $P_L(\mathrm{x})$ is the Legendre polynomial of order L, $(\Omega_k - \Omega_l)$ is the angle between the directions of vectors k and l in the same snapshot and the horizontal bar denotes averaging over all snapshots in the trajectory.

Matrix M was constructed for each trajectory using two sets of vectors. The initial set was composed of 40 vectors in each domain that could be assimilated to 'bond vectors' in the real structure and provided a good approximation to an isotropic angular distribution. The second set contained 38 additional vectors joining beads from different domains.

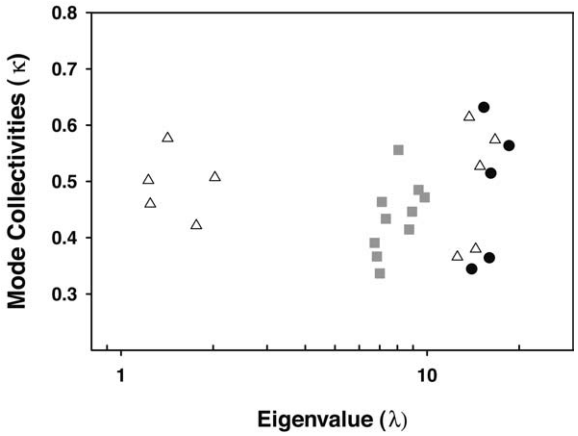

Figure 6. Mode collectivities, κ, *versus* eigenvalues λ for the modes with the largest eigenvalues for the 80 'bond-vector' set definition of matrix M and different values of K: 10 (circles), 0.025 (triangles), and 0.0025 (squares). The number of modes with large values of λ and their separation reflect the onset of inter-domain motion with decreasing values of K. Additional modes (not shown) have $\lambda < 0.1$ and reflect residual internal motion of the rigid model domains.

Diagonalization of M identifies the reorientation eigenmodes $|m\rangle$, with eigenvalues λ_m, each characterized by their collectivity κ which is a measure of the number of vectors that are significantly affected by each mode (Prompers et al., 2001).

Figure 6 shows plots of κ *versus* λ for the eigenmodes obtained from simulations carried out with multiple inter-domain contacts and different values of K. Table 2 shows the number of active reorientation modes and their separability.

For K values higher than 0.01, reorientation of rank 2 spherical harmonics is essentially described by only five modes, as expected for a rigid body. For lower K values the number of modes increases to ten and the gap between the first five modes, representing global motion, and the remaining five, which account for interdomain flexibility, decreases with the value of K. This gap is quantified by the separability parameter (Prompers and Brüschweiler, 2002b) showed in Table 2. For the lowest values of the force constant, internal and global reorientation modes are no longer separated. The small number of modes is consistent with the limited number of degrees of freedom of the model system in which internal mobility within each domain is totally restrained.

The contribution of individual vectors j by each reorientation mode m can be expressed in terms of principal order parameter components $\delta S^2_{j,m}$ (Prompers and Brüschweiler, 2002a)

$$\delta S^2_{j,m} = \lambda_m \left|\langle m|_j\right|^2. \tag{9}$$

Figure 7 shows the values of δS^2 corresponding to each vector for the ten reorientation modes obtained from a BD simulation with $K = 0.001$. The contribution of individual vectors to each mode depends on the set of vectors used as a base. When only 'local' vectors are considered, all modes contain contributions from the two domains. When long range, inter-domain vectors are added, some of the modes can be assigned to reorientation processes affecting individual domains. In this case, an eleventh mode (Mode 118), containing contributions solely from inter-domain vectors has the highest eigenvalue. Thus the use of inter-domain vectors provides a more intuitive picture of the complex motion in a two-domain protein. On the other hand, while 'local' vectors may be directly related to bond vectors, for which experimental information is directly accessible from heteronuclear relaxation experiments, the experimental counterpart of inter-domain vectors is much less apparent.

The last part of this work will be focused on the prediction of heteronuclear relaxation rates from BD simulations using the global reorientation modes derived from the set of 80 local vectors.

Correlation times and relaxation rates

The reorientation mode analysis does not consider the time sequence of the different conformations visited during the dynamics. The autocorrelation functions of the individual reorientation modes can be calculated from the time dependence of the projections of snapshots from BD simulation on each mode. The correlation functions were found to be mono-exponential to a good approximation and have converged at the end of the trajectory (Figure 8). The corresponding correlation times were obtained by fitting the decay of the autocorrelation function and from these the spectral density functions $J(\omega)$ of each local vector, j, could be computed using Equation 10

$$J_j(\omega) = \sum_m \delta S^2_{j,m} \frac{\tau_m}{1 + \omega^2 \tau_m^2}, \tag{10}$$

where the sum extends over all m active reorientation modes.

The dipole-dipole and chemical shift anisotropy contributions to heteronuclear relaxation rates can be calculated from the spectral density functions.

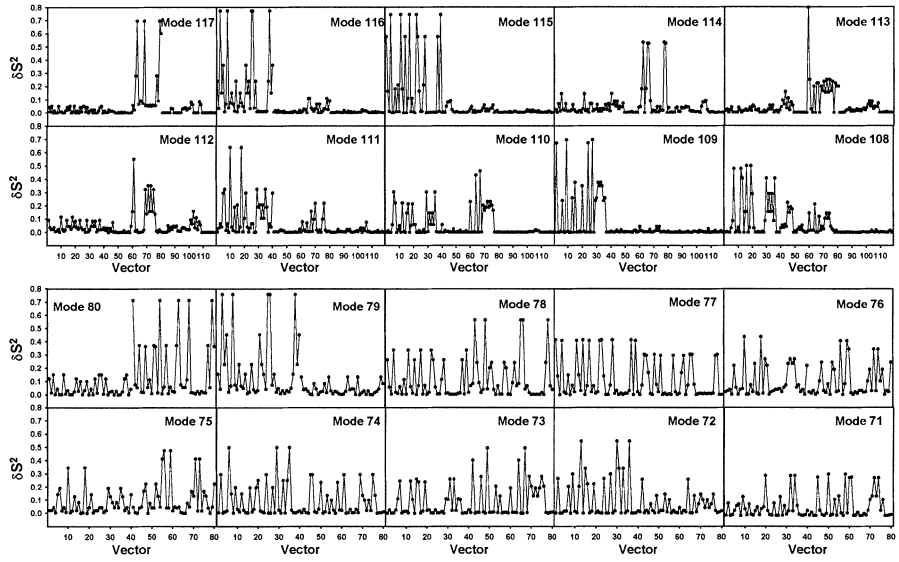

Figure 7. Vector contributions, δS^2, to active reorientational modes derived from the same BD simulation, with $K = 0.001$, using bases of 118 vectors, top panel, and 80 vectors, bottom panel. Vectors from 1 to 40 and from 41 to 80 vectors correspond to 'bond vectors' in the WW and catalytic domains respectively. Vectors from 81 to 118 in top panel correspond to inter-domain vectors that connect both domains.

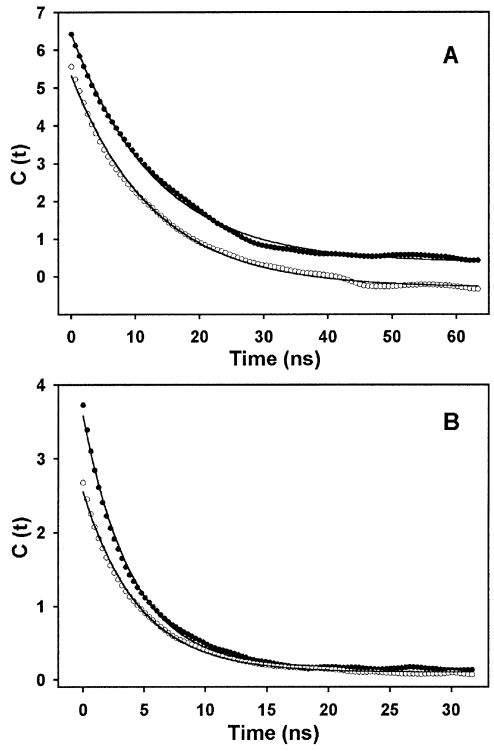

Figure 8. Autocorrelation functions of individual modes obtained from an iRED analysis of Brownian Dynamic simulations of model Pin1 with different values of K. Solid lines are the experimental fitting to the monoexponential decays. (A) $K = 10$. Mode 79 (closed circles) and 76 (open circles). (B) $K = 0.0025$. Mode 79 (closed circles) and 71 (open circles).

Figure 9 shows the values of R_2/R_1, calculated using different values of K, for a set of 80 NH vectors (NH distance 1.04 Å, CSA $= -160$ ppm), directed along the local vectors used to analyze the motion of model Pin1. While these vectors are not directly related to actual NH bonds in the real structure, the ensemble is representative and can be used to determine the expected dependence on inter-domain flexibility of the relaxation properties NH nuclei in a two-domain protein like Pin1.

Table 2 shows the average value of the ratio of relaxation rates, $<R_2/R_1>$, and their dispersion $(R_2/R_1)_{max}$-$(R_2/R_1)_{min}$ for the two domains, as a function of the flexibility parameter K. The calculated R_2/R_1 values show a strong dependence on inter-domain flexibility. When comparing the two largest values of K, increasing inter-domain flexibility results in a substantial decrease in R_2/R_1 values, suggesting shorter correlation times and an apparent lower molecular weight, in spite of the fact that only five reorientation modes are needed to describe the motion, suggesting a 'rigid body' behavior in both cases. This is in agreement with the results from rigid-body hydrodynamic calculations, using HydroNMR, that suggested that flexibility leads to apparent low values of the atomic element radius, a (Bernado et al., 2002).

As the flexibility increases, the average relaxation rates of the two domains become different, suggesting that they can be represented by two different correl-

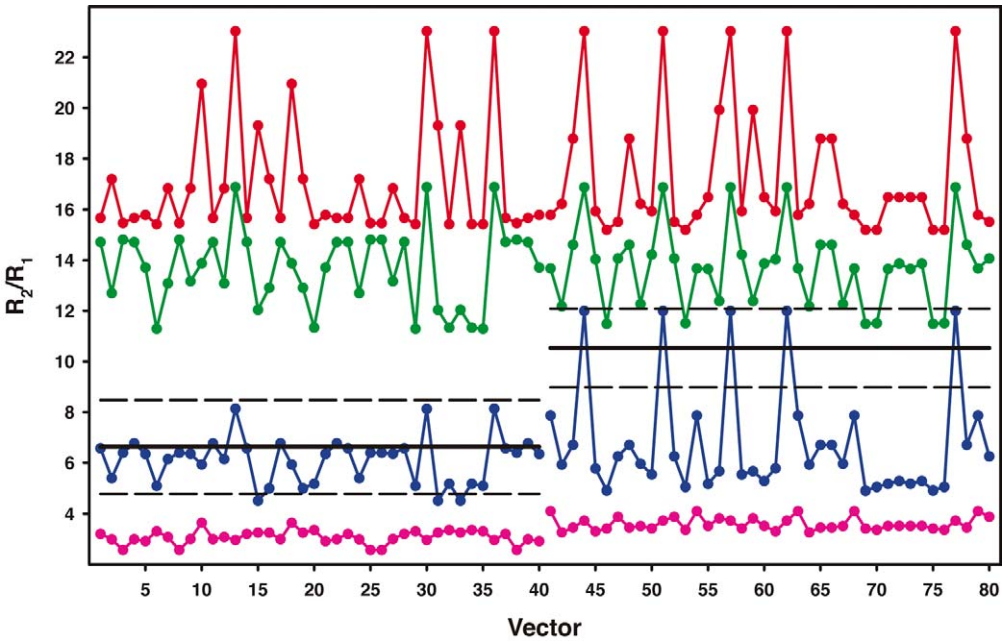

Figure 9. Calculated values of R_2/R_1 at 14.09 T for 80 hypothetical NH bonds directed along the 80 vectors used in the iRED analysis of BD simulations with K values of 10 (red), 0.025 (green), 0.01 (blue) and 0.001 (pink). The first 40 vectors belong to the WW domain and the last 40 vectors to the catalytic domain. Black horizontal lines show the average R_2/R_1 experimental value (solid lines), and the inter-residue dispersion (dashed lines) for each domain in a free Pin1 sample after excluding residues affected by exchange.

Table 2. Relaxation properties of the active modes for different values of K

K	Active modes	g_L	$<R_2/R_1>_{CD}$	R_2/R_1 $Disp_{CD}$	$<R_2/R_1>_{WW}$	R_2/R_1 $Disp_{WW}$
10	5	381.32	17.33	7.83	16.98	7.61
0.1	5	20.09	13.33	5.64	13.12	5.32
0.075	5	15.32	12.91	6.04	12.72	5.92
0.050	5	10.35	14.06	5.35	13.92	5.14
0.025	5	5.49	13.75	5.59	13.71	5.59
0.010	10	2.78	6.77	7.09	6.10	3.62
0.0075	10	2.54	5.96	3.99	5.30	1.88
0.0050	10	2.38	5.24	2.62	4.45	1.99
0.0025	10	2.28	4.33	1.64	3.63	1.37
0.0010	10	2.28	3.61	0.84	3.08	1.08

ation times. However, analysis of the reorientation modes clearly indicates that the mobility of the two domains is strongly correlated even for values of K as low as 0.001.

The decrease in R_2/R_1 as a function of K shows a sigmoidal behavior with a sharp drop around $K = 0.01$. This decrease is associated with the reduction of S^2_β and the increase in the inter-domain distance observed at the same K value and shows the onset of fast domain reorientation when direct domain-domain interactions are reduced.

The average experimental R_2/R_1 values of ^{15}N nuclei in the two domains of free Pin1 measured at 14.09 T are shown in Figure 9. The experimental values are in agreement with the expected values for the idealized model of Pin1 with $K = 0.01$. These values correspond to order parameters S^2_α and S^2_β of 0.76 and 0.18, respectively. This suggests that inter-domain motion has an important contribution to heteronuclear relaxation of free Pin1.

The apparent anisotropy, measured as the maximum difference in relaxation rates for residues be-

longing to the same domain but having different orientations, is also strongly dependent on inter-domain flexibility. However, anisotropy is clearly overestimated in our simplified model of Pin1 that does not consider inter-domain packing and its effect on the compensation of the intrinsic anisotropy of individual domains.

Concluding remarks

Brownian dynamic simulations of free Pin1 were performed on a highly idealized model. However, the cubes representing individual domains were parameterized so that they reproduce the hydrodynamic properties expected from the true three dimensional structures and Brownian Dynamic simulations are expected to faithfully reproduce the bulk dynamics. On the other hand, it is conceivable that the continuous interaction model, represented by the strings linking the two domains, really captures the essential feature that inter-domain interactions restrict inter-domain reorientation which is otherwise controlled by the hydrodynamic properties of individual domains while the long flexible linker plays only the role of keeping the domains within interaction distance but does not have much effect on the observed flexibility of Pin1. The good agreement between the calculated and observed average relaxation rates suggests that the model captures the essential effects of this flexible multi-domain protein, although the model is not unique.

Brownian Dynamic simulations provide, at a reasonable computational expense, a model for the extended global motion, including inter-domain reorientations, of two-domain proteins. If the real protein can be mapped on the simplified model used in BD simulations, the reorientation eigenmode analysis of the trajectories would provide a way to identify a reduced set of parameters that describe the overall motion and can be fitted to the experimental relaxation data. A description of the global properties of a rigid globular protein using an ideal ellipsoidal model has already proven to reproduce with good accuracy residual dipolar coupling data of individual NH bonds (Fernandes et al., 2001). Further experimental and computational work is still needed to validate and fully explore this possibility.

Supplementary material (available from the author)

Figure 1. Centre-to-centre inter-domain distances (A) and angles (B) in a 2 μs brownian dynamic simulations of an idealized Pin1 model including (black bars) or not (grey bars) hydrodynamic interactions.
Figure 2. (A) Definition of the dihedral angle in idealized model of free Pin1. (B) Distribution of the dihedral angle along a 2 μs brownian dynamic simulations of the axially restrained Pin1 model including (in black) or not (in red) the flexible linker. (C) Autocorrelation function in the rigid Pin1 mode, $K = 100$, of a vector parallel to the symmetry axis with (in black) or without (in red) flexible linker.

Acknowledgements

We gratefully acknowledge the help received from Dr Rafael Brüschweiler in the successful implementation of his iRED methodology. This work was supported by funds from the Spanish Ministerio de Ciencia y Tecnologia (BIO-2001-3115 and BQU2000-0029), the Generalitat de Catalunya (CERBA, Grup Consolidat i Xarxa Temàtica de RMN). PB was the recipient of a pre-doctoral grant from the Spanish MECD. MXF was the recipient of a postdoctoral fellowship from the Portuguese Foundation for Science and Technology.

References

Allen, M.P. and Tildesley, D.J. (1990) *Computer Simulations of Liquids*, Oxford, Claredon Press.
Antosiewicz, J. and McCammon, J.A. (1995) *Biophys. J.*, **69**, 57–65.
Antosiewicz, J., Briggs, J.M. and McCammon, J.A. (1996) *Eur. Biophys. J.*, **24**, 137–141.
Avigan, M.I., Stober, B. and Levens, D.A. (1990) *J. Biol. Chem.*, **265**, 18538–18545.
Baber, J., Szabo, A. and Tjandra, N. (2001) *J. Am. Chem. Soc.*, **123**, 3953–3959.
Bernadó, P., Åkerud, T., García de la Torre, J., Akke, M. and Pons, M. (2003) *J. Am. Chem. Soc.* **125**, 916–923.
Bernadó, P., García de la Torre, J. and Pons, M. (2002) *J. Biomol. NMR*, **23**, 139–150.
Braddock, D.T., Louis, J.M., Baber, J.L., Levens, D. and Clore, M.G. (2002) *Nature*, **415**, 1051–1056.
Brune, D. and Kim, S. (1994) *Proc. Natl. Acad. Sci. USA*, **91**, 2930–2934.
Brüschweiler, R., Liao, X. and Wright, P. (1995) *Science*, **268**, 886–889.
Burd, C.G. and Dreyfuss, G. (1994) *Science*, **265**, 615–621.
Campbell, I.D. and Downing, A.K. (1998) *Nat. Struct. Biol.*, **5**, 496–499.

Carrasco, B. and García de la Torre, J. (1999a) *Biophys. J.*, **75**, 3044–3057.

Carrasco, B. and García de la Torre, J. (1999b) *J. Chem. Phys.*, **110**, 4817–4826.

Chang, S.-L. and Tjandra, N. (2001) *J. Am. Chem. Soc.*, **123**, 11484–11485.

Chou, J.J., Li, S., Klee, C.B. and Bax, A. (2001) *Nat. Struct. Biol.*, **8**, 990–997.

Clore, G.M., Szabo, A., Bax, A., Kay, L.E., Driscoll, P.C. and Gronenborn, A.M. (1990) *J. Am. Chem. Soc.*, **112**, 4989–4991.

Dagget, V. (2000) *Curr. Opin. Struct. Biol.*, **10**, 160–164.

Ermak, D.L. and MacCammon, J.A. (1978) *J. Chem. Phys.*, **69**, 1352–1360.

Fernandes, M.X., Bernadó, P., Pons, M. and García de la Torre, J. (2001) *J. Am. Chem. Soc.*, **123**, 12037–12047.

Fischer, M.W.F., Losonczi, J.A., Weaver, J.L. and Prestegard, J.H. (1999) *Biochemistry*, **38**, 9013–9022.

Fushman, D., Xu, R. and Cowburn, D. (1999) *Biochemistry*, **38**, 10225–10230.

García Bernal, J.M. and García de la Torre, J. (1980) *Biopolymers*, **19**, 751–766.

García de la Torre, J. and Bloomfield, V.A. (1981) *Q. Rev. Biophys.*, **14**, 81–139.

García de la Torre, J., Huertas, M.L. and Carrasco, B. (2000) *J. Magn. Reson.*, **147**, 138–147.

Gerstein, M. and Krebs, W. (1998) *Nucl. Acids Res.*, **26**, 4280–4290.

Ikura, M., Clore, G.M., Gronenborn, A.M., Zhu, G., Klee, C.B. and Bax, A. (1992) *Science*, **256**, 632–638.

Iniesta, A. and García de la Torre, J. (1990) *J. Chem. Phys.*, **92**, 2015–2018.

Jacobs, D.M., Saxena, K., Vogtherr, M., Bernadó, P., Pons, M. and Fiebig, K. (2003) *J. Biol. Chem.*, **278**, 26174–26182.

Levitt, M. (1976) *J. Mol. Biol.*, **104**, 59–107.

Lipari, G. and Szabo, A. (1982a) *J. Am. Chem. Soc.*, **104**, 4546–4559.

Lipari, G. and Szabo, A. (1982b) *J. Am. Chem. Soc.,* **104**, 4559–4570.

Lu, K.P., Liou, Y.-C. and Zhou, X.Z. (2002) *Trends Cell Biol.*, **12**, 164–172.

Meador, W.E., Means, A.R. and Quiocho, F.A. (1993) *Science*, **262**, 1718–1721.

Peter, C., Daura, X. and van Gunsteren, W.F. (2001) *J. Biomol. NMR*, **20**, 297–310.

Prompers, J.J. and Brüschweiler, R. (2001) *J. Am. Chem. Soc.*, **123**, 7305–7313.

Prompers, J.J. and Brüschweiler, R. (2002a) *J. Am. Chem. Soc.*, **124**, 4522–4534.

Prompers, J.J. and Brüshweiler, R. (2002b) *Proteins*, **46**, 177–189.

Prompers, J.J., Lienin, S.F. and Brüschweiler, R. (2001) In *Biocomputing: Proceedings of the 2001 Pacific Symposium*, Altman, R.B., Dunker, A.K., Hunter, L., Lauderdale, K. and Klein, T.E., World Scientific, Singapore, pp. 79–88.

Ranganathan, R., Lu, K.P., Hunter, T. and Noel, J.P. (1997) *Cell*, **89**, 875–886.

Rotne, J. and Prager, J. (1969) *J. Chem. Phys.*, **50**, 4831–4837.

Sekerina, E., Rahfeld, J.U., Müller, J., Fanghänel, C.R., Fischer, G. and Bayer, P.J. (2000) *Mol. Biol.*, **301**, 1003–1017.

Sicheri, F. and Kuriyan, J. (1997) *Curr. Opin. Struct. Biol.*, **7**, 777–785.

Tjandra, N., Garrett, D.S., Gronenborn, A.M., Bax, A. and Clore, G.M. (1997) *Nat. Struct. Biol.*, **4**, 443–449.

Tolman, J.R., Flanagan, J.M., Kennedy, M.A. and Prestegard, J.H. (1995) *Proc. Natl. Acad. Sci. USA*, **92**, 9279–9283.

Varadan, R., Walker, O., Pickart, C. and Fushman, D. (2002) *J. Mol. Biol.*, **324**, 637–647.

Verdecia, M.A., Bowman, M.E., Lu, K.P., Hunter, T. and Noel, J.P. (2000) *Nat. Struct. Biol.*, **7**, 639–643.

Wade, R.C., Davies, M.E., Luty, B.A., Madura, J.D. and McCammon, J.A. (1993) *Biophys. J.*, **64**, 9–15.

Yamakawa, H. (1970) *J. Chem. Phys.*, **53**, 436–443.

Yuan, X., Werner, J.M., Lack, J., Knott, V., Handford, P.A., Campbell, I.D. and Downing, A.K. (2002) *J. Mol. Biol*, **316**, 113–125.

Zhou, X.Z., Lu, P.-J., Wulf, G. and Lu, K.P. (1999) *Cell. Mol. Life Sci.*, **56**, 788–806.